ARTICLE

Characterization of freeze-dried oxidized human red blood cells for pre-transfusion testing by synchrotron FTIR microspectroscopy live-cell analysis

Received 00th January 20xx,
Accepted 00th January 20xx

DOI: 10.1039/x0xx00000x

Thulya Chakkumpulakkal Puthan Veettil[a,b#], Diana Alves[c#] , Jitraporn Vongsvivut[d], Rosemary L Sparrow [e], Bayden R Wood[a]* and Gil Garnier[c]*

ABSTRACT: Oxidative treatment of human red blood cells (RBCs) prior to freeze-drying appears to stabilize the RBCs to withstand dried storage at room temperature. To better understand the effects of oxidation and freeze-drying/rehydration on RBC lipids and proteins, single-cell measurements were performed by synchrotron-based Fourier transform infrared (FTIR) microspectroscopy 'live-cell' (unfixed) analysis. Lipid and protein spectral data of tert-butyl hydroperoxide (TBHP)-oxidized RBCs (oxRBCs), FDoxRBCs and control (untreated) RBCs were compared using principal component analysis (PCA) and band integration ratios. The oxRBCs and FDoxRBCs samples had similar spectral profiles that were clearly different to control RBCs. Spectral changes in the CH stretching region of oxRBCs and FDoxRBCs indicated the presence of increased saturated and shorter-chain lipids, consistent with lipid peroxidation and stiffening of the RBC membrane compared to control RBCs. The PCA loadings plot for the fingerprint region of control RBCs corresponding to the α–helical structure of hemoglobin, shows that oxRBCs and FDoxRBCs have conformational changes in the protein secondary structure to β-pleated sheets and β-turns. Finally, the freeze-drying process did not appear to compound or induce additional changes. In this context, FDoxRBCs could become a stable source of reagent RBCs for pre-transfusion blood serology testing. The synchrotron FTIR microspectroscopic live-cell protocol provides a powerful analytical tool to characterize and contrast the effects of different treatments on RBC chemical composition at the single cell level.

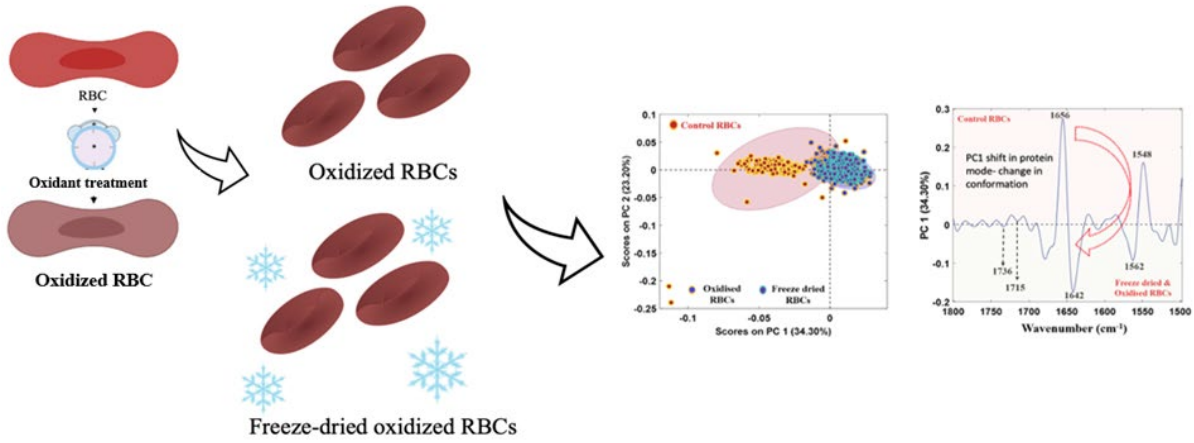

[a] Centre for Biospectroscopy, Monash University, Clayton, Victoria 3800, Australia
[b] Centre for Sustainable and Circular Technologies (CSCT), University of Bath, BA2 7AY, United Kingdom (U.K)
[c] Bioresource Processing Research Institute of Australia (BioPRIA), Department of Chemical and Biological Engineering, Monash University, Clayton, Victoria 3800, Australia
[d] Infrared Microspectroscopy (IRM) beamline, ANSTO–Australian Synchrotron, Clayton, Victoria 3168, Australia
[e] Transfusion Research Unit, Department of Epidemiology and Preventive Medicine, School of Public Health and Preventive Medicine, Monash University, Melbourne, Victoria 3004, Australia
equal first authors
*E-mails: gil.garnier@monash.edu, bayden.wood@monash.edu

Introduction

Current sources of reagent red blood cells (RBCs) used for pre-transfusion blood group serology testing are supplied in liquid form, which has significant practical limitations, including short shelf-life and the need for continual refrigeration. Freeze-drying has the potential to be an efficient process to enable longer-term room temperature storage of reagent RBCs. However, freeze-drying can damage RBCs due to low-temperature stress, ice crystallization, pH changes and dehydration stress.[1] Typically, cryoprotectants are used

to mitigate damage to cells caused by ice nucleation during freezing.[2] Efforts to develop effective freeze-drying protocols to preserve RBCs together with cryoprotectants have been hindered by poor RBC recovery rates following cell rehydration.[3] In the process of addressing these limitations, we made an interesting discovery that a pre-freeze oxidation step, without the need of a cryoprotectant, appears to stabilize the RBC membrane and maintains intact RBCs throughout the subsequent freeze-drying and rehydration steps (Alves, manuscript in preparation). Although it is known that oxidative stress modifies the chemical composition of the RBC membrane and cytoskeleton leading to rigidification and alteration in cell mechanical properties,[4, 5] the effect of oxidation in combination with freeze-drying of RBCs has not been investigated. The blood group alloantigens typed in pre-transfusion tests are defined by variations in amino acid sequence or carbohydrates present on glycoproteins or glycolipids at the external cell surface;[6] therefore a detailed understanding of the chemical changes that occur at the RBC membrane following oxidation and freeze-drying is important. Furthermore, the conformational structure and orientation of RBC alloantigens are influenced by changes in membrane fluidity caused by alternations to surrounding membrane lipids and the unique cytoskeletal protein network of RBCs.[7] Label-free single-cell chemical mapping, as is possible by Fourier transform infrared (FTIR) microspectroscopy, would achieve the level of sub-cellular precision needed to assess chemical changes at the RBC surface membrane.[8, 9]

FTIR microspectroscopy has been used in a wide variety of biological applications, including chemical mapping of changes to blood cells such as malaria-infected RBCs, hematological diseases and blood diagnostics.[10-14] The precision and versatility of FTIR-microspectroscopy is further enhanced when coupled with a synchrotron radiation energy source that significantly intensifies the beamline, facilitating 'live-cell' analyses, i.e. cells suspended in physiological medium.[15-17] Herein, we aim to better understand the effects of oxidation and freeze-drying/rehydration on the human RBC membrane by determining changes in spectral data generated from synchrotron FTIR microspectroscopy 'live-cell' analysis of single RBCs.

Experimental Section

Materials.

Phosphate buffered saline (PBS) (pH 7.2), tert-butyl hydroperoxide (TBHP), polystyrene petri dishes (60 x 15 mm) and microcentrifuge tubes (1.5 mL) were from Sigma-Aldrich (St. Louis, MO). RBC preservative solution (Celpresol) (pH 7.2) was from Immulab, Melbourne, Australia, and 0.9% (w/v) NaCl solution was from Baxter, Deerfield, IL. CaF_2 windows (0.5 mm-depth) were from Crystran (Poole, UK).

RBC samples.

EDTA-anticoagulated whole blood samples from healthy volunteer donors, screened negative for Hepatitis B and C, HIV, and syphilis were provided by Australian Red Cross Lifeblood (Melbourne, Australia). The blood samples were stored at 4°C and used within 7 days after blood donation. RBCs were isolated by centrifugation at 75 x *g* for 2 minutes at 22°C in a microcentrifuge, washed three times in PBS and resuspended in RBC preservation solution at a final concentration of 1% of cells (v/v) (equates to approximately $5x10^7$ RBCs/mL).

Oxidation treatment of RBCs.

For oxidation treatment, RBCs were incubated in the presence of 0.5 mM TBHP oxidant (final concentration) for 35 minutes in a 37°C water bath (henceforth referred to as oxRBCs). Control RBCs were incubated under identical conditions, except without TBHP (henceforth referred to as control RBCs). After incubation the samples were washed three times in PBS after treatment and resuspended in RBC preservative solution at a final concentration of 1% of cells (v/v).

Freeze-drying of oxRBCs and rehydration.

For freeze-drying, the 1% (v/v) oxRBC suspension was pipetted into microcentrifuge tubes (150 µL/tube), covered with punctured parafilm, and placed in an open plastic bag. The tubes were placed in liquid nitrogen for 1-2 minutes to snap-freeze the RBCs, and then transferred to a laboratory-scale freeze-dryer (beta 1-8 LDplus, Christ, Berlin, Germany) and freeze-dried for 2.5 hours under vacuum at 0.03 mBar (0.003 kPa). The freeze-dried samples were kept at ambient temperature for 24 h before rehydration.

After freeze-drying, the samples were rehydrated by dropwise addition of RBC preservative solution at room temperature at a rate of 60 drops/min, with gentle mixing by tapping the tube until complete homogenisation (henceforth referred to as FDoxRBCs). FDoxRBCs were washed six times with 0.9% NaCl at 75 x *g* for 2 minutes in a microcentrifuge and finally resuspended in 1 mL of 0.9% NaCl.

RBC sample preparation for spectral measurement.

To prepare 'live-cell' RBC samples for spectroscopic analysis, 25 µL of 0.06% (v/v) RBCs suspended in 0.9% NaCl were placed onto the centre of 0.5 mm-depth CaF_2 windows and dispersed by orbital movement with the assistance of tweezers. A clean CaF_2 window was placed on the top of the suspension to prevent moisture evaporation. The spectral data were acquired on selected single cells within 3 – 4 min time intervals before the saline solution completely dries out. New sample aliquots were loaded with same concentration in each time.

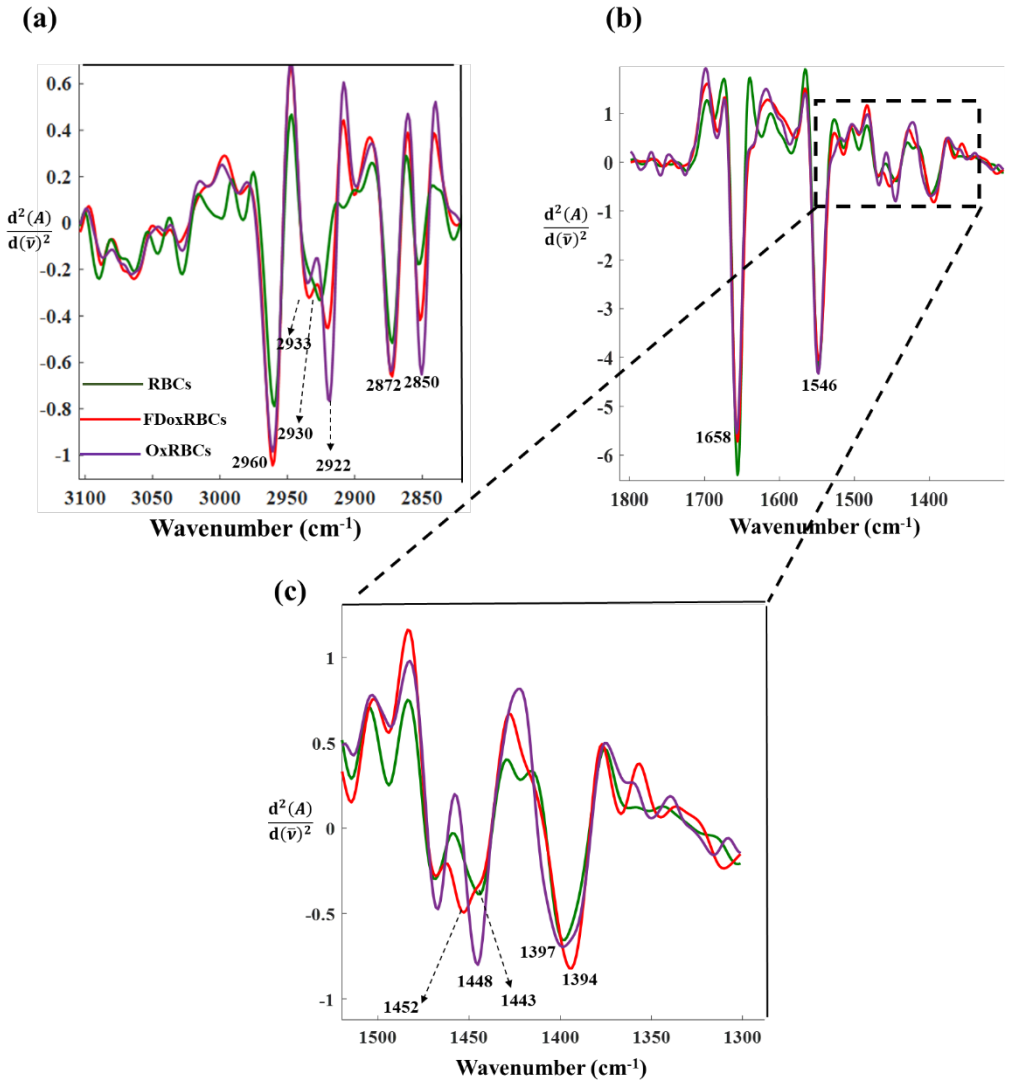

Figure 1: A) Second derivative vector normalized spectra of RBC, oxRBCs, and FDoxRBCs in: A) CH stretching region (3100 – 2800 cm^{-1}). B) fingerprint region (1800 – 1300 cm^{-1}). C) Magnified view of 1500 – 1300 cm^{-1} fingerprint regions.

Synchrotron FTIR mapping measurement of single RBCs.

All spectral measurements of the RBC samples were recorded on the Infrared Microspectroscopy (IRM) beamline at the Australian Synchrotron (Clayton, Victoria, Australia). A Bruker V80v FTIR spectrometer coupled with a Hyperion 3000 FTIR microscope, and a liquid nitrogen cooled narrow-band mercury cadmium telluride detector was utilised in transmission mode using a matching 36× objective and condenser (NA, 0.50) (Bruker Optik GmbH, Ettlingen, Germany). Spectra were acquired within the 4000 – 1000 cm^{-1} spectral region. For all samples, 64 co-added scans were employed with a projected aperture of 5.6 µm. The spectra of 100 single RBCs/sample were recorded for subsequent analysis. For the 'live-cell' samples, a background spectrum of 128 co-added scans was recorded through the surrounding 0.9% NaCl medium within the same CaF_2 substrates. Blackman-Harris 3-Term apodization, Mertz phase correction, and zero-filling factor of 2 were set as default acquisition parameters using OPUS 8.0 software suite (Bruker Optik GmbH). The spectra were 'atmospheric corrected' for water and CO_2 using OPUS 8.0 software (Bruker Optik GmbH). By recording spectra in an aqueous medium, Mie scattering and the artefacts generated by the refractive index are minimized because the refractive index of the 0.9 % NaCl solution (n = 1.33) is very close to that of cells (n = ~1.37).[18, 19] Furthermore, by using the second derivative spectra in the modelling minimises baseline aberrations caused by Mie scattering and other non-specific matrix absorbances.

Resonant Mie scattering (RMieS) – Extended multiplicative scattering correction (EMSC) of recorded spectra

The biological cells or tissues often encounters issues related to significant baseline distortions owing to the scattering effects, especially resonant Mie scattering (RMieS). This can cause shift in apparent peak positions and significant peak distortions. Bassan *et al.* developed an algorithm to correct such 'dispersion artefacts' in

the recorded spectra.[20, 21] Herein, we have utilized the modified RMieS-EMSC algorithm (version 5, RMieS_EMSC_v5) to correct the data for Mie scattering effects reported elsewhere.[20] As a reference spectrum, we have used the mie scatter free average spectrum from red blood cells and single iteration was performed on the raw data. The lower range of the scattering particle radius value is taken as 2 µm and the upper range of the scattering particle radius value is taken as 12 µm. All analysis was carried out using MATLAB software (MathWorks, Natick, MA) using the modified codes reported in the literature.[20] Mie scatter corrected spectra were used for further analysis.

Spectral data pre-processing and multivariate analysis.

Spectroscopic data were analysed using MATLAB software aided with PLS-Toolbox (Eigenvector Research Inc., Manson, WA). PLS-Toolbox was used for importing and pre-processing the data for multivariate data analysis. The Savitzky–Golay algorithm was employed for computing the second derivative of the spectra (15-point smoothing window and 2nd order polynomial) followed by standard normal variate (SNV) normalization. PCA is a statistical technique that aims to reduce the dimensionality of a data set. It is particularly useful for complex and large datasets, by projecting the maximum variance among them. PCA, a dimension reduction strategy, was performed on the second derivative (19-point smoothing window and 2nd order polynomial function), vector normalized spectra followed by mean centring. Outlier correction was done prior to the decomposition analysis.

One-way Analysis of Variance (ANOVA)

Statistical analysis by one-way ANOVA was carried out on the lipid and protein band ratios using GraphPad Prism software (San Diego, CA, U.S.A). For ANOVA, the four different biochemical entities (i.e., CH_2 asymmetric stretching band/total lipid, Lipid/protein, Amide II/I, and Unsaturated/saturated lipid) were individually selected as the dependent variables and the three different RBC treatments (RBCs, FDoxRBCs, and oxRBCs) were the independent variables. Statistical significance was defined as p value < 0.0001.

Results and Discussion

Live-cell analysis of RBCs.

The second derivative vector normalized spectra from 'live-cell' RBC measurements are shown in Figure 1. Figure S1 represents the baseline corrected average spectra from RBCs, OxRBCs, and FDoxRBCs. The band at 2922 cm^{-1}, due to the asymmetric CH_2 acyl chains lipids, has become relatively intensified in oxRBCs and FDoxRBCs compared to control RBCs. The CH_2 symmetric stretching mode from acyl chain lipids, which can be observed around cm^{-1} is more enhanced in oxRBCs and FDoxRBCs compared to control RBCs. The degree of saturation is enhanced in oxidized RBCs due to lipid peroxidation. This finding indicates that TBHP-induced oxidation converts unsaturated lipids to saturated lipids, thereby influencing the membrane fluidity and bilayer thickness.[22] The second derivative spectra of control RBCs, oxRBCs and FDoxRBCs is divided into lipid

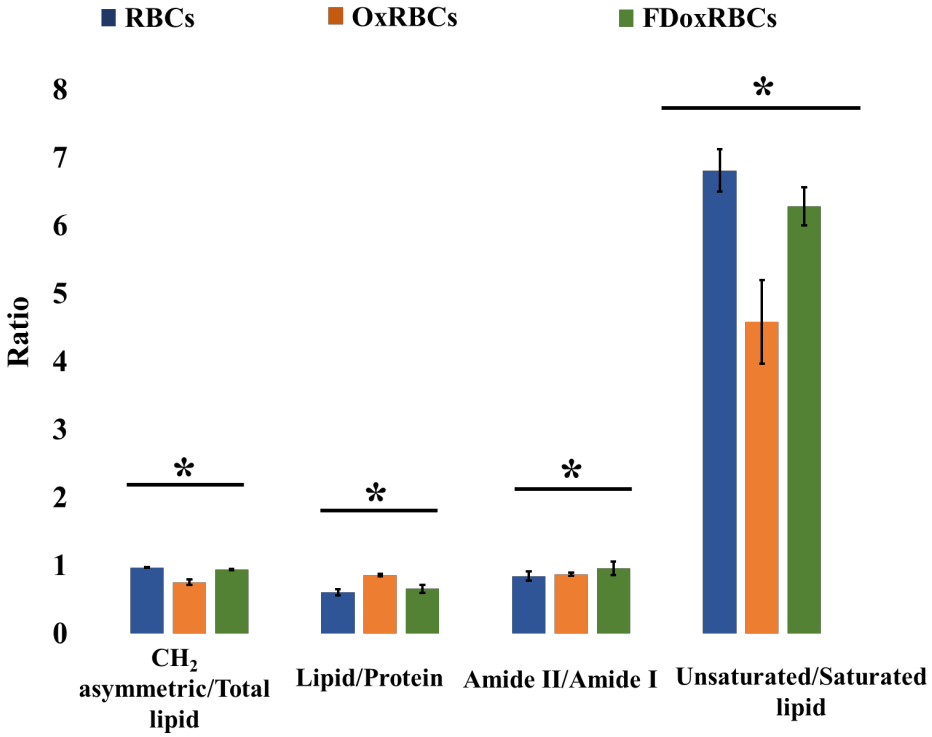

Figure 2. Calculated integrated area ratios of lipid and protein spectral bands for RBCs, oxRBCs and FDoxRBCs. The effect of the RBC treatments is statistically significantly different (*p value of < 0.0001 by one-way ANOVA) for each of the lipid and protein ratio entities.

(3100 – 2800 cm^{-1}, Figure 2a) and fingerprint regions (1800 – 1300 cm^{-1}, Figure 2b). Figure 2c is a magnification of the 1500 – 1300 cm^{-1} fingerprint region with bands labelled. An intense Amide I band 1658 cm^{-1} arises from the C=O stretching of the peptide backbone. The intensity of this band has slightly increased in control RBCs, whilst smaller bands at ~1450 cm^{-1} and ~1400 cm^{-1} corresponding to the bending vibrations of CH_2 and CH_3 groups from lipid chains and proteins are more intense in oxRBCs (1448 and 1397 cm^{-1}) and FDoxRBCs (1452 and 1394 cm^{-1}).[23] Table 1 lists the important bands and their corresponding wavenumber values in the IR spectra of functional RBCs.

The determination of lipid and protein band ratios.

To better elucidate the composition of lipids and proteins in cells, the integrated area under the particular lipid or protein band was calculated, and the integrated peak ratios determined. Figure 2 shows the ratios of lipid bands between the conditions. Evaluation by one-way ANOVA shows that for each of the ratio configurations, the effects of the RBC treatments are statistically significantly different ($p < 0.0001$). In detail, the sum of integrated intensities of CH_2 asymmetric and symmetric stretching bands (2950 – 2900 cm^{-1} and 2860 – 2840 cm^{-1} regions, respectively), which corresponds to the saturated lipids provides an indicator of the total lipid content in the cell samples.[24] The integrated area ratio of CH_2 asymmetric stretching band to the total lipid was calculated to obtain information about qualitative lipid acyl chain lengths.[24] The ratio is higher in control RBCs compared to oxRBCs and FDoxRBCs ($p < 0.0001$). Hence shorter-chain lipids are primarily present in oxRBCs and FDoxRBCs, whilst control RBCs contain more long-chain lipids compared to the other cell groups analysed. The relative elevated saturated lipid content in oxRBCs and FDoxRBCs indicates a higher number of hydrogen bonds, which would contribute to higher membrane rigidity.[25] The ratio of the integrated area for the 2919 cm^{-1} (2950 – 2900 cm^{-1} region) and 2850 cm^{-1} (2860 – 2840 cm^{-1} region) bands in oxRBCs and FDoxRBCs complements the results shown in the second derivative spectra (i.e., Figure 1a). Similarly, the unsaturated lipid content was calculated by integrating the area between 3100 – 3000 cm^{-1} in the raw spectra.[24] The unsaturated/saturated lipid ratio was calculated by taking the ratio of the area of the olefinic band (~3012 cm^{-1}) to the sum of the saturated lipid bands[24]. This ratio is significantly reduced in FDoxRBCs and oxRBCs compared to control RBCs ($p < 0.0001$), and is consistent with a decrease in double bonds in the lipid structures of the oxidized RBCs. This may be due to the decrease in the olefinic content in the cellular lipid membrane of oxRBCs and FDoxRBCs, which is consistent with increased lipid peroxidation.

Hemoglobin (Hb) is the main protein in RBCs.[26] Changes in the secondary structure of Hb from α-helical to unordered conformations under oxidative conditions have been identified.[27]. Moreover, disordered protein organization involved formation of β-sheets and a decrease in α-helices related to the aggregation process stabilized by strong intermolecular hydrogen bonding at the secondary structure level. A previous study reported that storage of packed RBCs resulted in a gradual increase in the irreversible changes in the secondary and quaternary structures of Hb, with subsequent impairment of the T↔R transition.[28] This manifests as an increase in the ratio of the amide II/amide I bands for the oxRBC and FDoxRBCs, as shown in Figure 2. To further interrogate the data, another PCA model was built in the fingerprint region (1800 – 1500 cm^{-1}). The amide II band at 1551 cm^{-1} from N–H bending vibrations and C–N vibrations of the peptide group is enhanced in control RBCs. This finding is corroborated by the fact that the protein to lipid ratio is higher in control RBCs (Figure 2). The 1685 cm^{-1} band in negative loadings corresponds to the β-turn secondary structure of proteins, indicating an increase in the number of intramolecular hydrogen bonds. β-turns arise mainly due to the tendency to form intramolecular hydrogen bonds.[29] Although C=O stretching from the ester carbonyl band (at 1740 cm^{-1}) appears in the negative loadings, the maximum variance among the RBC groups is principally due to the protein conformational changes.

Variance between different treatments of RBCs using PCA.

The PCA modelling demonstrates the alteration in structural-configurational of proteins and membrane phospholipids (Figure 3 & 4). The investigation of the differences between control RBC, oxRBCs and FDoxRBCs was performed by applying PCA on the FTIR spectra of

Wavenumber (cm^{-1})	Band assignment	Entity
3012	Olefinic C=CH stretching vibration	Lipids
2960	Asymmetric CH_3 acyl chains	Lipids
2922	Asymmetric CH_2 acyl chains	Lipids
2872	Symmetric CH_2 acyl chains	Lipids
2850	Symmetric CH_2 acyl chains	Lipids
1658	Amide I	Proteins
1546	Amide II	Proteins
1740 & 1725	n(C=O) ester carbonyl	Lipids
1765	n(C=O) ester carbonyl	Lipids

Table 1. Notable IR spectral bands.

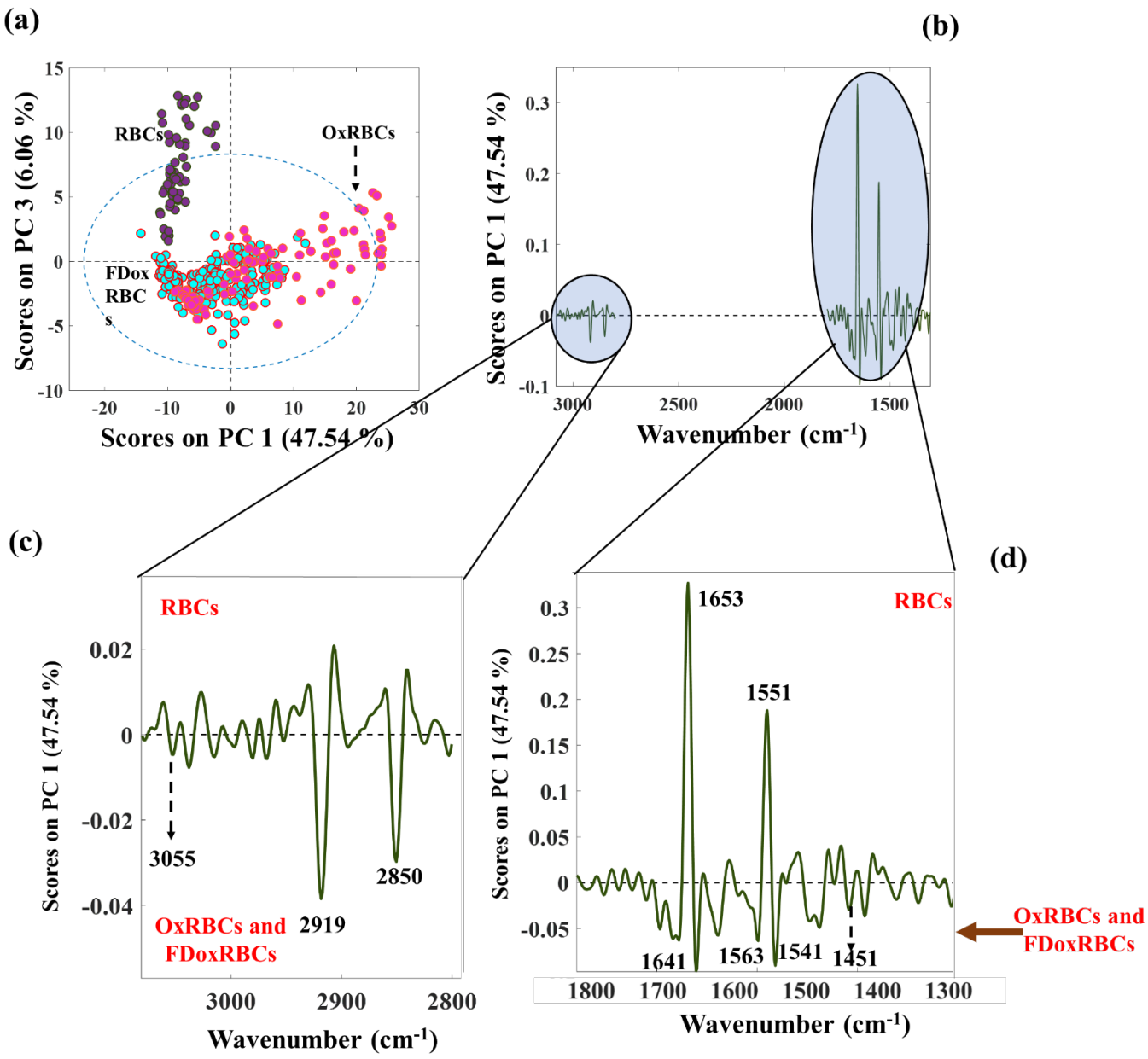

Figure 3: Identification of chemical similarities and differences between RBC treatments by PCA. a) PC1 vs PC3 2D-scores plot of the 3100 – 1300 cm^{-1} region, showing clusters of the RBC (purple), oxRBC (pink), and FDoxRBC (sky blue). b) Corresponding PC1 loading plot of 3100 – 1300 cm^{-1} region. c) magnified view of the loadings plots in the 3100 – 2800 cm^{-1} region and d) 1800 – 1300 cm^{-1} region. The clustering of spots is indicative of their similarity.

RBCs in their aqueous state. Principal components are created to capture the amount of variation in the data. For example, the first PC (PC1) will detect the maximum variance direction in the data, and is essentially a line that best accounts for the majority of variance in the data set. Therefore, PCA provides an insight into the similarities and differences in chemical composition between control RBCs, oxRBCs, FDoxRBCs, as distinguished by the different colored clusters shown in Figure 3a over 3100 – 1300 cm^{-1} region. Furthermore, the loadings plot PC1 supports the second-derivative spectra (Figure 3c & d).

OxRBCs and FDoxRBCs were clustered together and separated from the control RBCs, indicating that oxRBCs and FDoxRBCs are chemically similar. The distinct separation or maximum variance between control RBCs, oxRBCs and FDoxRBCs occurred along PC1 (47.54%) in a 2D-score plot based on the 3100 – 1300 cm^{-1} region. Since the PCA was performed on the second derivatized data, the positive scores are associated with negative loadings and *vice versa*. The bands responsible for the separation correspond to the swarm of data points depicted in the loadings plot in Figure 3c & d. It is evident that both symmetric and asymmetric CH_2 acyl chains lipidic activities (observed at 2919 cm^{-1} and 2850 cm^{-1} which are attributed to the presence of CH_2 asymmetric and symmetric stretch from lipids and fatty acids, respectively) are intense in oxRBCs and FDoxRBCs groups compared to control RBCs (Fig. 3c & d). Similarly, the degree of unsaturation is increased in the FDox and OxRBCs groups, which is

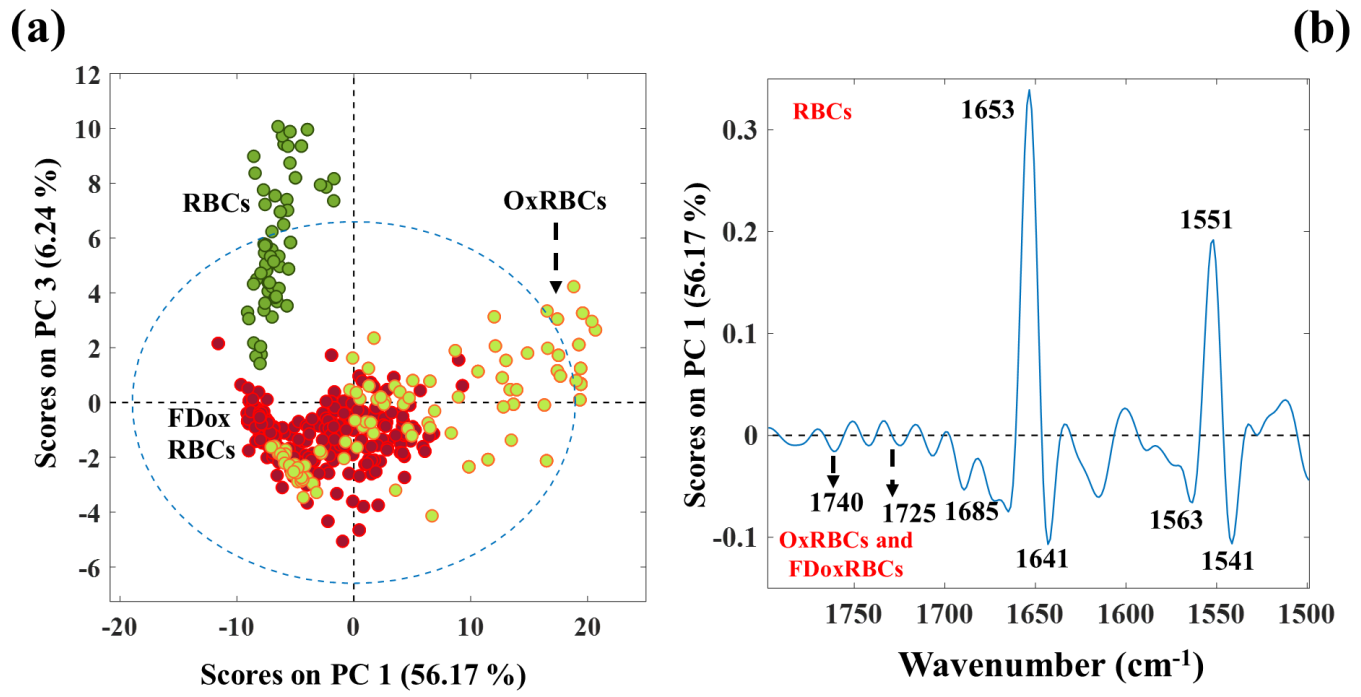

Figure 4: a) Score plot of the 1800 – 1500 cm^{-1} region and b) corresponding loadings plot

evident by the presence of intense 3055 cm^{-1} (due to olefinic C- H stretching due to unsaturated fatty acid chains) band in the negative PC1 loadings. These results indicate the higher lipid susceptibility to oxidation. The band at 1451 cm^{-1} is due to the bending vibrations of CH_2 groups from lipid chains and proteins. As demonstrated in the second derivative spectra, this band is enhanced in the FDoxRBCs and OxRBCs group in PC1 loadings plot. Similarly, the scores plot of PCA in the region 1800 – 1500 cm^{-1} is depicted in Figure 4a. The spectral similarities between oxRBCs and FDoxRBCs suggest that the freeze-drying process does not affect the oxRBC characteristics. The band at 1653 cm^{-1} in control RBCs corresponds to the α–helical structure and is shifted to 1641 cm^{-1} consistent with random coil structures in oxRBCs and FDoxRBCs. It is indicative of conformational change in the protein secondary structure to β-pleated sheets and β-turns (Figure 4b). This protein conformational change is further confirmed in Figure 4b PC1 loadings plot, which shows a shift in the protein mode from 1653 cm^{-1} (control RBC) to 1641 cm^{-1} (oxRBC and FDoxRBC). As evidenced from the PC1 vs PC3 scores plot, the distinct differentiation between FDoxRBCs and OxRBCs and RBCs is enhanced along PC1 vs PC3 plot. This is confirmed by the presence of intensified negative PC1 loadings peaks including 3055 cm^{-1}, 2919 cm^{-1}, 2850 cm^{-1}, 1641 cm^{-1}, and 1451 cm^{-1} from the FDoxRBCs and OxRBCs groups.

Conclusion

Using the exquisite sensitivity of synchrotron FTIR microspectrometry, the effects of TBHP-oxidation and freeze-drying/rehydration treatments on the chemical composition of human RBCs were identified. To our knowledge, this is the first report of such an analysis. Live-cell analysis conditions were advantageous to obtain spectral data on RBCs suspended in a natural state in physiologically aqueous medium, as previously reported for other cell types.[16] Consistent with lipid peroxidation, oxRBCs and FDoxRBCs had more short-chain lipids and decreased olefinic content compared to control RBCs. The conversion of unsaturated lipids to saturated lipids and increased hydrogen bonds in oxRBCs and FDoxRBCs are consistent with increased cell rigidity, which is a known consequence of oxidative stress.[25] Furthermore, TBHP-oxidation caused a loss of protein content and changes in the secondary structure of Hb, from α-helical to unordered conformations consisting of β-pleated sheets and β-turns. PCA analysis confirmed that oxRBCs and FDoxRBCs are chemically similar indicating that freeze-drying/rehydration does not induce additional changes to the oxRBCs. Overall, the results indicate higher susceptibility of RBC lipids to TBHP-oxidation. As demonstrated here, the synchrotron FTIR microspectroscopy protocol provides a powerful analytical tool to characterize and contrast the effects of different treatments on RBC chemical composition at the single cell level. This will greatly benefit our endeavour to discover the optimal preservation strategy to enable long-term room temperature storage of human RBCs suitable for use as reagents in pre-transfusion testing and diagnostics. To this end, the finding that freeze-drying does not induce additional changes to the TBHP-oxidized RBCs is insightful, and provides a baseline to investigate other potential agents or treatment conditions that can stabilize RBCs to withstand dried storage at room temperature, while preserving intact, morphologically normal RBC and their membrane alloantigenic structures.

Author Contributions

All authors contributed to the study and the preparation of the manuscript. All authors have approved the final version of the manuscript. #Authors TCPV and DA contributed equally.

Conflict of interest

The authors declare that the research was conducted without any commercial or financial relationships that could be construed as a potential conflict of interest.

Ethical statement

De-identified human blood samples were provided by the Australian Red Cross Lifeblood, with approval from their Human Research Ethics Committee. This study was approved by the Monash University Human Research Ethics Committee.

Acknowledgements

This study was performed on the IRM beamline at Australia Synchrotron (Victoria, Australia), ANSTO. The use of IRM was funded as part of the Projects at the Australian Synchrotron (Project ID: M17147) and has been made available to users of the IRM Beamline. TCPV is a recipient of an Australian Institute of Nuclear Science and Engineering (AINSE) postgraduate research award (PGRA) 2021. We thank Dr. Keith Bambery and Callum Gassner for their valuable suggestions on resonant mie scattering correction algorithm. This work was funded in part by the Australian Research Council (ARC) and Haemokinesis Ltd (Melbourne, Australia) through a linkage program, grant, LP160100544.

References

1. V. Rindler, S. Lüneberger, P. Schwindke, I. Heschel and G. Rau, *Cryobiology*, 1999, **38**, 2-15.
2. G. D. Elliott, S. Wang and B. J. Fuller, *Cryobiology*, 2017, **76**, 74-91.
3. D. Alves, R. Sparrow and G. Garnier, *Journal of Biomedical Materials Research Part B: Applied Biomaterials*, 2021, **109**, 1689-1697.
4. S. I. Rizvi and P. K. Maurya, *Annals of the New York Academy of Sciences*, 2007, **1100**, 373.
5. I. Cicha, Y. Suzuki, N. Tateishi and N. Maeda, *Pathophysiology (Amsterdam)*, 1999, **6**, 103-110.
6. M. E. Reid and N. Mohandas, 2004.
7. N. Yeow, R. F. Tabor and G. Garnier, *Advances in Colloid and Interface Science*, 2017, **249**, 149-162.
8. L. M. Miller and P. Dumas, *Biochimica et Biophysica Acta (BBA)-Biomembranes*, 2006, **1758**, 846-857.
9. A. Marcelli, A. Cricenti, W. M. Kwiatek and C. Petibois, *Biotechnology advances*, 2012, **30**, 1390-1404.
10. G. T. Webster, K. A. De Villiers, T. J. Egan, S. Deed, L. Tilley, M. J. Tobin, K. R. Bambery, D. McNaughton and B. R. Wood, *Analytical Chemistry*, 2009, **81**, 2516-2524.
11. C. Sandt, O. Feraud, M.-L. Bonnet, C. Desterke, R. Khedhir, S. Flamant, C. G. Bailey, J. E. Rasko, P. Dumas and A. Bennaceur-Griscelli, *Biochemical and biophysical research communications*, 2018, **503**, 1861-1867.
12. M. Grigoruţă, A. Vargas-Caraveo, E. Vázquez-Mayorga, H. A. Castillo-Michel, Á. G. Díaz-Sánchez, J. Reyes-Herrera and A. Martínez-Martínez, *Spectrochimica Acta Part A: Molecular and Biomolecular Spectroscopy*, 2018, **204**, 475-483.
13. K. Kochan, D. E. Bedolla, D. Perez-Guaita, J. A. Adegoke, T. C. P. Veettil, M. Martin, S. Roy, S. Pebotuwa, P. Heraud and B. R. Wood, *Applied Spectroscopy*, 2021, **75**, 611-646.
14. K. P. P. R. Nair, T. C. P. Veettil, B. R. Wood, D. Paul and T. Alan, *Biosensors*, 2022, **12**, 119.
15. C. Petibois, M. Piccinini, M. C. Guidi and A. Marcelli, *Journal of synchrotron radiation*, 2010, **17**, 1-11.
16. J. Doherty, A. Raoof, A. Hussain, M. Wolna, G. Cinque, M. Brown, P. Gardner and J. Denbigh, *Analyst*, 2019, **144**, 997-1007.
17. I. Delfino, V. Ricciardi and M. Lepore, *Applied Sciences*, 2021, **12**, 336.
18. D. R. Whelan, K. R. Bambery, L. Puskar, D. McNaughton and B. R. Wood, *Analyst*, 2013, **138**, 3891-3899.
19. Y. Sung, W. Choi, C. Fang-Yen, K. Badizadegan, R. R. Dasari and M. S. Feld, *Optics express*, 2009, **17**, 266-277.
20. P. Bassan, A. Kohler, H. Martens, J. Lee, H. J. Byrne, P. Dumas, E. Gazi, M. Brown, N. Clarke and P. Gardner, *Analyst*, 2010, **135**, 268-277.
21. P. Bassan, A. Sachdeva, A. Kohler, C. Hughes, A. Henderson, J. Boyle, J. H. Shanks, M. Brown, N. W. Clarke and P. Gardner, *Analyst*, 2012, **137**, 1370-1377.
22. Á. Catalá, *Front Physiol*, 2015, **6**, 520-520.
23. T. Bebesi, D. Kitka, A. Gaál, I. C. Szigyártó, R. Deák, T. Beke-Somfai, K. Koprivanacz, T. Juhász, A. Bóta and Z. Varga, *Scientific reports*, 2022, **12**, 1-13.
24. D. Yonar, L. Ocek, B. I. Tiftikcioglu, Y. Zorlu and F. Severcan, *Scientific reports*, 2018, **8**, 1-13.
25. J. M. Kwan, Q. Guo, D. L. Kyluik-Price, H. Ma and M. D. Scott, *American journal of hematology*, 2013, **88**, 682-689.
26. R. Malka, F. F. Delgado, S. R. Manalis and J. M. Higgins, *PLoS Comput Biol*, 2014, **10**, e1003839-e1003839.
27. A. Blat, J. Dybas, M. Kaczmarska, K. Chrabaszcz, K. Bulat, R. B. Kostogrys, A. Cernescu, K. Malek and K. M. Marzec, *Analytical chemistry*, 2019, **91**, 9867-9874.
28. E. Szczesny-Malysiak, J. Dybas, A. Blat, K. Bulat, K. Kus, M. Kaczmarska, A. Wajda, K. Malek, S. Chlopicki and K. M. Marzec, *Biochimica et Biophysica Acta (BBA)-Molecular Cell Research*, 2020, **1867**, 118803.
29. N. Panasik Jr, P. J. Fleming and G. D. Rose, *Protein science*, 2005, **14**, 2910-2914.

